
FROM EMBEDDINGS TO ACCURACY: COMPARING FOUNDATION MODELS FOR RADIOGRAPHIC CLASSIFICATION

Xue Li¹, Jameson Merkow², Noel C. F. Codella², Alberto Santamaria-Pang²,
 Naiteek Sangani², Alexander Ersoy², Christopher Burt², John W. Garrett¹, Richard J. Bruce¹,
 Joshua D. Warner¹, Tyler Bradshaw¹, Ivan Tarapov², Matthew P. Lungren², Alan B. McMillan¹

¹University of Wisconsin–Madison, Madison, WI USA

²Microsoft Health and Life Sciences, Redmond, WA USA

ABSTRACT

Foundation models, pretrained on extensive datasets, have significantly advanced machine learning by providing robust and transferable embeddings applicable to various domains, including medical imaging diagnostics. This study evaluates the utility of embeddings derived from both general-purpose and medical domain-specific foundation models for training lightweight adapter models in multi-class radiography classification, focusing specifically on tube placement assessment. A dataset comprising 8,842 radiographs classified into seven distinct categories was employed to extract embeddings using six foundation models: DenseNet121, BiomedCLIP, Med-Flamingo, MedImageInsight, Rad-DINO, and CXR-Foundation. Adapter models were subsequently trained using classical machine learning algorithms, including K-Nearest Neighbors (KNN), logistic regression (LR), Support Vector Machines (SVM), random forest (RF), and Multi-Layer Perceptron (MLP). Among these combinations, MedImageInsight embeddings paired with an SVM adapter yielded the highest mean area under the curve (mAUC) at 93.8%, followed closely by Rad-DINO (91.1%) and CXR-Foundation (89.0%). In comparison, BiomedCLIP and DenseNet121 exhibited moderate performance with mAUC scores of 83.0% and 81.8%, respectively, whereas Med-Flamingo delivered the lowest performance at 75.1%. Notably, most adapter models demonstrated computational efficiency, achieving training within one minute and inference within seconds on CPU, underscoring their practicality for clinical applications. Furthermore, fairness analyses on adapters trained on MedImageInsight-derived embeddings indicated minimal disparities, with gender differences in performance within 2% and standard deviations across age groups not exceeding 3%. These findings confirm that foundation model embeddings—especially those from MedImageInsight—facilitate accurate, computationally efficient, and equitable diagnostic classification using lightweight adapters for radiographic image analysis.

Keywords Foundation Models · Embedding · Adapter Training · Radiographic Image Classification

1 Introduction

Radiography remains an essential diagnostic imaging modality, playing a critical role in clinical decision-making, procedural guidance, and patient monitoring [1]. Accurate interpretation of radiographs, especially for verifying correct tube placement, is directly tied to patient safety and treatment outcomes, as misplacement can lead to severe complications [2, 3]. Despite its importance, radiology faces an increasing burden due to the immense volume of imaging studies. In the United States alone, approximately 5,000 radiologists are tasked with interpreting over 126 million radiographic examinations each year [4]. This heavy workload can strain radiologists, potentially impacting diagnostic accuracy, efficiency, and overall patient care quality.

In recent years, artificial intelligence (AI) and machine learning (ML) have been progressively integrated into radiological practice to enhance diagnostic accuracy and workflow efficiency [5, 6, 7]. Despite these promising developments, the implementation of end-to-end deep learning models in clinical practice often faces significant challenges. They

inherently require task-specific training [8]. Consequently, whenever a new clinical condition or classification task arises, developing and training an entirely new model becomes necessary. Additionally, these approaches face significant challenges in generalizing across different sites due to variations in imaging protocols and equipment, which shift data distributions [9, 10]. As a result, each medical site typically needs to independently train new models, an approach that is both resource-intensive and inefficient. These limitations underscore the urgent need for more flexible and resource-efficient solutions.

More recently, foundation models represent a significant advancement in artificial intelligence, characterized by large-scale architectures pre-trained through self-supervised learning on extensive, multimodal datasets [11, 12, 13]. A primary strength of foundation models is their ability to produce generalizable embeddings which capture a compact, high-dimensional representation that is rich with meaningful information from input data. These embeddings can be efficiently adapted or fine-tuned for a wide range of downstream tasks, eliminating the need to train entirely new models from scratch [14, 15, 16]. Consequently, integrating foundation model embeddings with traditional machine learning classifiers presents a novel and promising approach in radiographic image analysis [17]. Utilizing these robust feature representations, conventional machine learning classifiers such as k-nearest neighbors (KNN), logistic regression (LR), support vector machines (SVM), random forests (RF), and multi-layer perceptrons (MLP) can be effectively optimized for multi-class classification. Preliminary results indicate that this integration can achieve high mean area under the curve (mAUC) metrics [15, 18, 19], demonstrating strong potential in detecting subtle radiographic variations essential for accurate tube placement verification. Nevertheless, a systematic evaluation comparing embeddings derived from general-purpose versus medical domain-specific models is critical to determine the most effective embedding strategy.

This study seeks to address this gap by systematically assessing the performance of various foundation model embeddings in training lightweight adapter classifiers for multi-class classification of radiography images. By focusing on tube placement, a task with significant clinical implications, we aim to determine the optimal combinations that not only enhance diagnostic accuracy but also ensure computational efficiency. The evaluation spans multiple models and classifiers, providing a comprehensive comparison that reflects the diverse capabilities of current foundation models in a clinically relevant setting. We hypothesize that these embeddings will enable high diagnostic performance while maintaining the computational efficiency necessary for real-time clinical deployment.

2 Materials and Methods

2.1 Study Design and Dataset

This study was designed to evaluate the performance of lightweight adapter models trained on embeddings derived from pre-trained foundation models for the multi-class classification of radiography images, with a focus on tube placement verification. The dataset, summarized in Fig. 1, comprises 8,842 radiographs that had been previously labeled into seven diagnostic categories by human readers. The seven diagnostic classes analyzed in this study encompass endotracheal tube (ETTube, 5.9%) and nasogastric tube (NGTube, 30.3%) placements, a normal radiographic study (NormalStudy, 13.4%), and three critical pathological findings—air in the peritoneal cavity (pneumoperitoneum, 5.5%), air in the pleural space (pneumothorax, 5.5%), and rib fractures (RFracture, 13.6%)—along with the presence of a vascular line (VLine, 25.8%), such as a central venous catheter or peripherally inserted central catheter (PICC line). These classes are relatively uncommon in public datasets, making this dataset well-suited for evaluating the generalization capabilities of foundation model embeddings. The images were retrospectively collected, encompassing a diverse range of patient demographics and imaging device manufacturers, as illustrated in Fig. 1. The dataset includes radiographs from patients across various age groups, with a higher proportion in the 40–80 age range, and imaging data acquired from multiple manufacturers, including Philips, Fujifilm, and Kodak, among others. This diversity ensures a broad representation of clinical scenarios relevant to tube placement assessment. Due to the retrospective nature of this study, a waiver of informed consent was obtained.

2.2 Image Preprocessing and Embedding Extraction

Each radiograph underwent a standardized preprocessing protocol to ensure uniformity across the dataset. Initially, the images were normalized by rescaling pixel intensities to a fixed range of 0 to 255. This normalization step was critical to minimize variations due to differing acquisition parameters and to facilitate a consistent input format for subsequent processing. The normalized images were then passed through six distinct pre-trained foundation models—DenseNet-121 [20], BiomedCLIP [15], Med-Flamingo [21], MedImageInsight [19], Rad-DINO [22], and CXR-Foundation[18]—to extract high-dimensional feature embeddings as shown in Phase 1 of Fig. 2. These models, pre-trained on large-scale datasets, functioned as automated feature extractors, generating representations that capture the intricate structural and textural details of the radiographs. DenseNet was sourced from *timm* [23] and the remaining models from HuggingFace [24, 25, 26, 27, 28]. Embedding extraction was performed using the default configurations

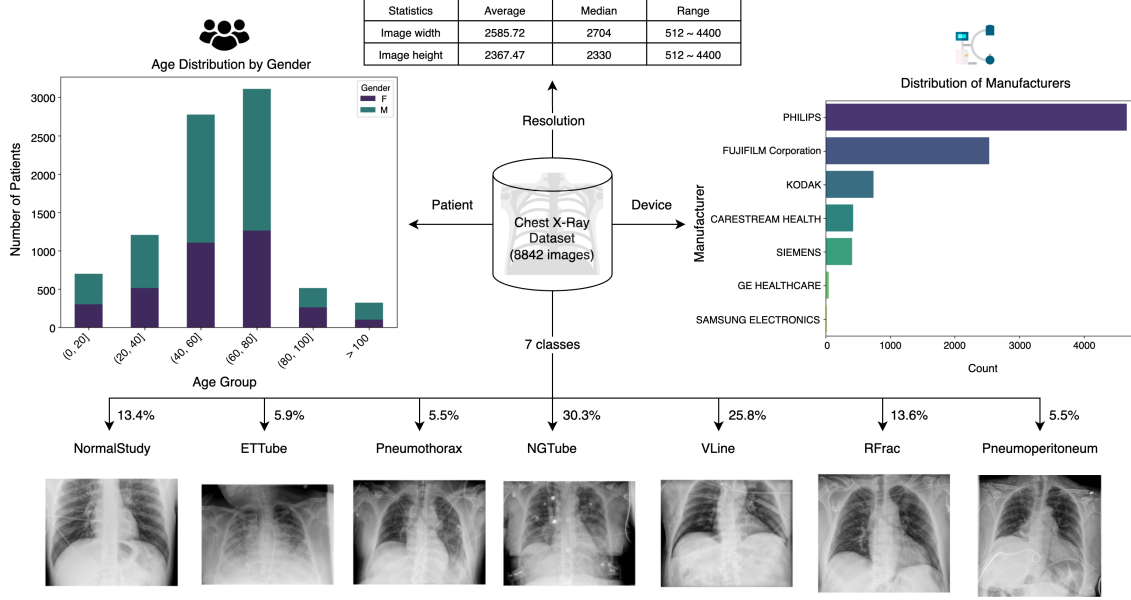


Figure 1: Overview of the Chest X-ray dataset used in this study. The dataset comprises 8,842 radiographs, categorized into seven diagnostic classes: NormalStudy (13.4%), ETTube (5.9%), Pneumothorax (5.5%), NGTube (30.3%), VLine (25.8%), RFrac (13.6%), and Pneumoperitoneum (5.5%). (**Left**) The age distribution of patients, stratified by gender. (**Right**) The distribution of imaging device manufacturers. (**Top**) Summary of image resolution statistics.

provided by each model’s developers to maintain consistency and reproducibility across the embedding extraction pipeline. The embedding length is 512 for BiomedCLIP; 768 for Med-Flamingo and Rad-DINO; and 1024 DenseNet-121, MedImageInsight, and CXR-Foundation. To analyze the learned representations from each foundation model before adapter training, t-SNE [29] was applied to the extracted embeddings for visualization.

2.3 Adapter Model Training and Optimization

The resulting feature embeddings served as inputs for training a series of lightweight adapter classifiers as illustrated in Phase 2 of Fig. 2. The dataset was partitioned into three non-overlapping subsets: a training set, a validation set, and an independent test set with ratios of 64%, 16%, and 20%, respectively. The training set was employed to fit various traditional machine learning classifiers using *scikit-learn*[30]: K-nearest neighbors (KNN), logistic regression (LG), support vector machines (SVM), random forest (RF), and multi-layer perceptron (MLP). For each classifier, hyperparameter optimization was carried out using the validation set. This optimization process involved systematic adjustments to key parameters—such as the number of neighbors in the KNN algorithm, optimization methods in the LG algorithm, kernel functions and its degree in SVM, tree depth and number of trees in the RF, and the architectural parameters in the MLP—to maximize performance. Once the optimal hyperparameters were determined, the final models were retrained on the training data with the optimal hyperparameters before being evaluated on the test set.

2.4 Performance Evaluation

Model performance was primarily evaluated using the mAUC, calculated for each combination of foundation model embeddings and lightweight adapter models. For a comprehensive assessment, additional metrics—including accuracy, precision, recall, and F1 score—were computed for each diagnostic class using the best-performing embedding-adapter combination, defined by the highest overall mAUC. To facilitate deeper insights into classification performance, confusion matrices were generated to visualize class-specific predictions and to identify frequent misclassification patterns.

Beyond overall accuracy, fairness was systematically analyzed across gender and age groups for the optimal embedding model combined with various adapter configurations. Specifically, area under the curve (AUC) scores were calculated separately for females (709 patients) and males (1059 patients), as well as across five distinct age brackets: (0, 20], (20, 40], (40, 60], (60, 80], and (80, 100] with 164, 237, 570, 610, and 99 patients respectively. Patients older than 100 were unidentified and were excluded from analysis. Additionally, computational efficiency was evaluated by measuring

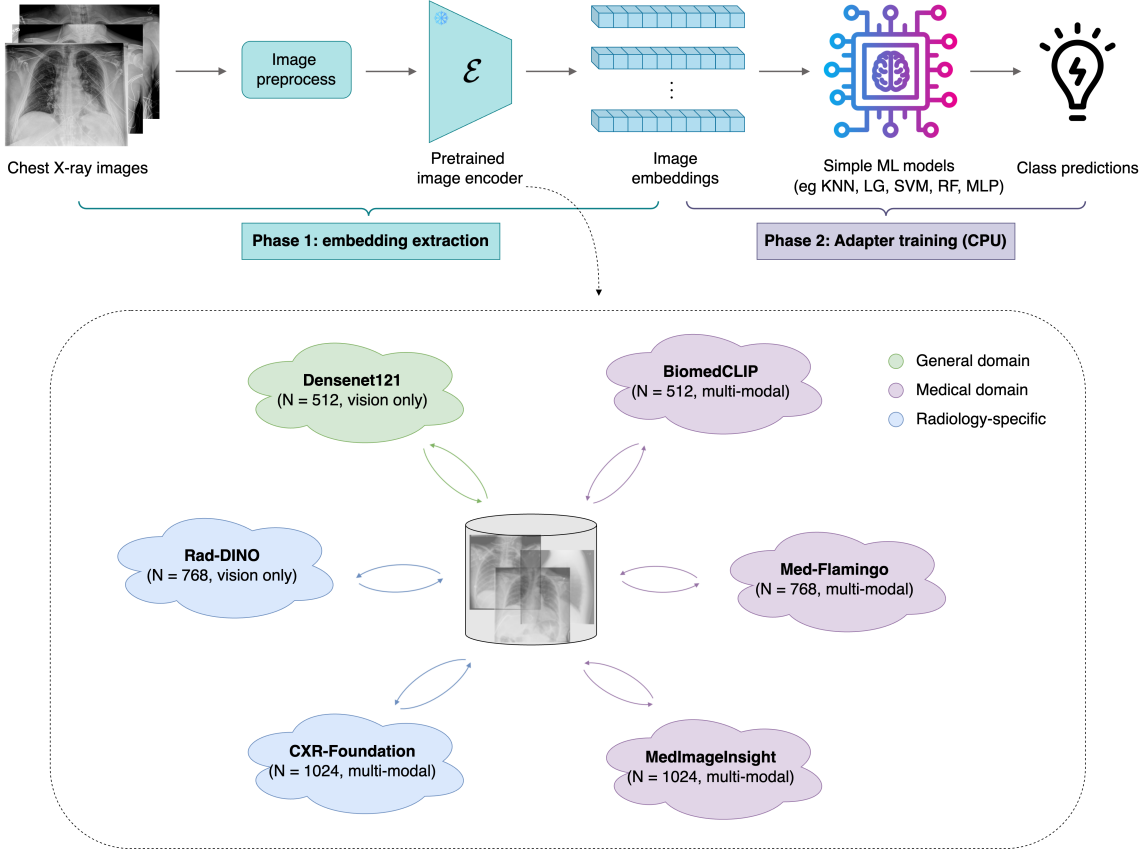


Figure 2: Two-phase workflow for radiograph classification. Phase 1: Embedding Extraction—Chest X-ray images were preprocessed and passed through pre-trained foundation models, including DenseNet121, BiomedCLIP, Med-Flamingo, MedImageInsight, Rad-DINO, and CXR-Foundation, to generate image embeddings. Phase 2: Adapter Training—Embeddings were used as input to lightweight ML models for class prediction, enabling efficient transfer learning.

training and inference times (in seconds) for each adapter model executed on a CPU. These efficiency measurements underscore the lightweight nature of the adapters, highlighting their suitability for rapid deployment, particularly in resource-constrained environments.

This evaluation framework rigorously validates the hypothesis that foundation model embeddings can effectively train lightweight adapters for multi-class radiograph classification, ensuring high diagnostic accuracy, computational efficiency, and equitable performance across demographic groups, thus supporting reliable and fair clinical practice.

3 Results

A total of 8,842 radiographs were analyzed, each labeled into one of seven diagnostic categories relevant to tube placement verification. These images were first processed and then fed into the pre-trained foundation models. The visualization of the embeddings from six foundation models involved in this study is shown in Fig. 3. The clustering patterns highlighted each model’s ability to differentiate diagnostic categories within the embedding space. Notably, MedImageInsight embeddings exhibited distinct separation across several clinical categories, indicating their effectiveness in capturing subtle yet critical visual differences essential for accurate radiographic classification. Similarly, CXR-Foundation embeddings demonstrated promising clustering patterns, with observable transitions between classes. In contrast, embeddings from other models lacked clear separation, suggesting differences in how each model encodes radiographic features.

Once the embeddings were extracted, lightweight adapters were trained on CPU for radiographic classification. The classification performance of all combinations of foundation model embeddings and lightweight adapter models was evaluated using mAUC, as shown in Fig. 4. Across configurations, the adapters exhibited a range of diagnostic

Comparing Foundation Models for Radiographic Classification

performance, with notable variation driven by the choice of foundation model embeddings. Among the six foundation models, MedImageInsight consistently achieved the highest overall mAUC across adapter types, with top performance from SVM (93.8%), followed closely by MLP (93.7%) and LR (93.5%). In contrast, Med-Flamingo produced the lowest mAUC scores, with all adapters falling below 78%, reflecting its limited suitability for this task and highlighting the variability in embedding quality across foundation models.

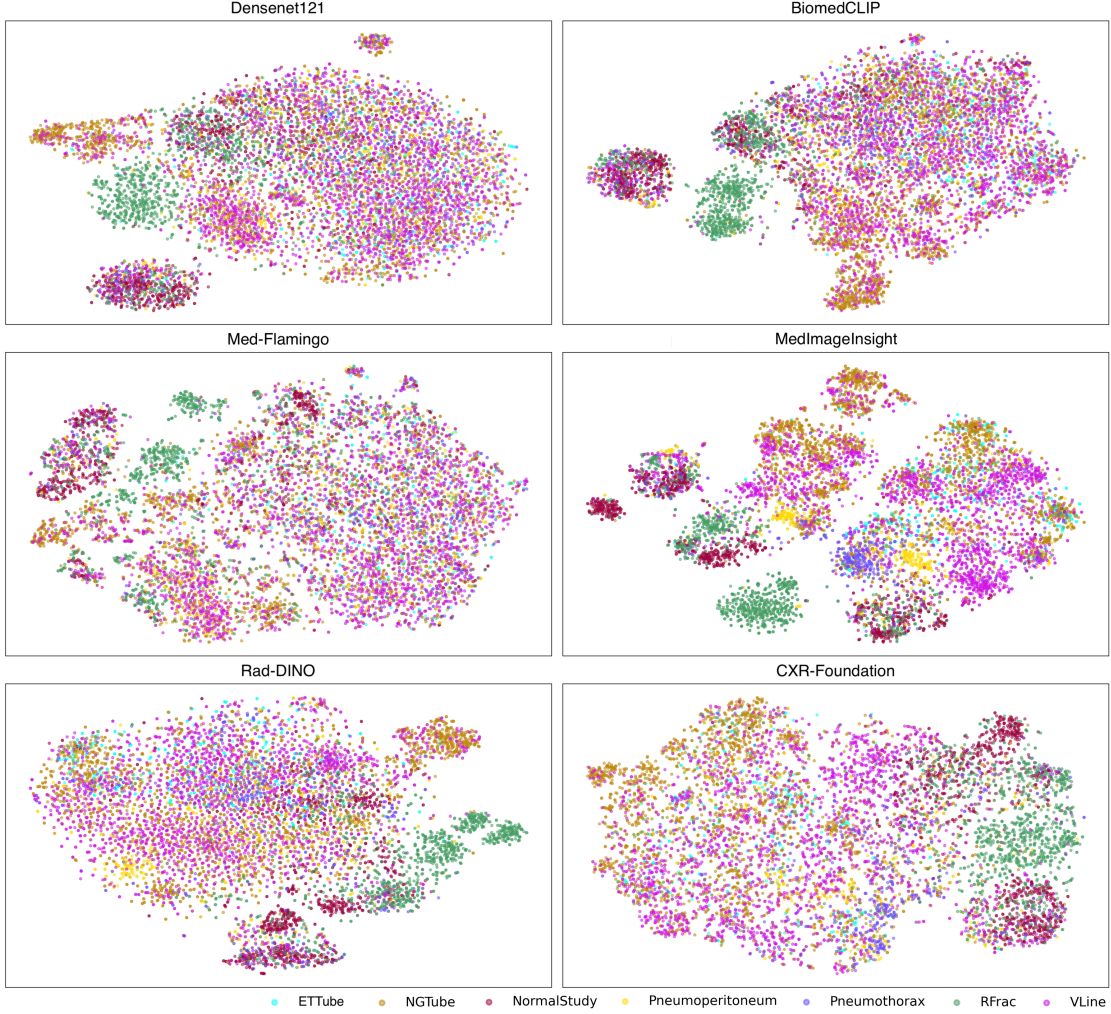


Figure 3: t-SNE visualization of embeddings extracted from six foundation models: DenseNet121, BiomedCLIP, Med-Flamingo, MedImageInsight, Rad-DINO, and CXR-Foundation. Each point represents a radiograph, color-coded according to its diagnostic category: ETTube, NGTube, NormalStudy, Pneumoperitoneum, Pneumothorax, RFrac, and VLine.

When evaluating foundation models, a clear trend emerges along the spectrum from general to domain-specific. DenseNet121, originally trained on broad natural image datasets, demonstrated moderate performance (mAUC range: 76.5%–81.8%). Models with some biomedical adaptation, like BiomedCLIP (trained on scientific figure–caption pairs, mAUC 79.1%–83.0%), showed incremental improvements but remained limited for this specific radiographic task. Surprisingly, Med-Flamingo, another medical domain-adapted model trained on scientific image–text pairs, only achieved an mAUC of 70.5%–77.5%, which is worse than DenseNet121. In contrast, models more closely aligned with radiographic imaging outperformed these approaches: Rad-DINO (focused on radiography images, mAUC 86.4%–91.1%) and CXR-Foundation (specialized in chest X-rays, mAUC 86.6%–89.0%). Notably, MedImageInsight—though not tailored to any single task—achieved the highest mAUC of 93.8%, likely owing to its broad domain-specific training across multiple medical imaging modalities.

From an adapter model perspective, SVM consistently outperformed other methods across six of the seven foundation models, underscoring its strong compatibility with high-dimensional embeddings. MLP and RF also delivered

Comparing Foundation Models for Radiographic Classification

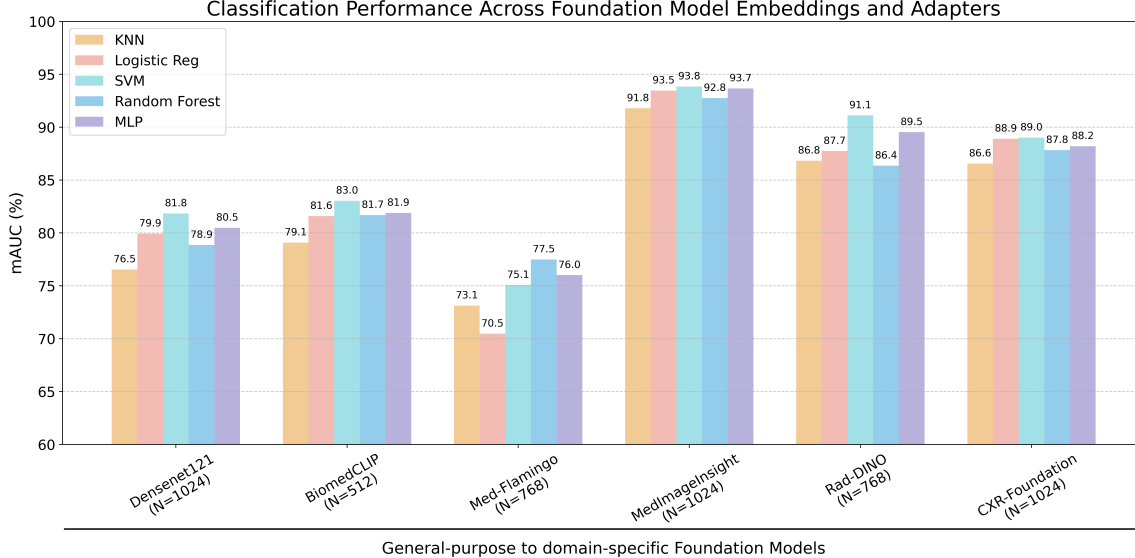


Figure 4: Performance comparison of adapter models (KNN, LR, SVM, RF, and MLP) paired with embeddings from general-purpose to domain-specific foundation models, evaluated by mAUC. N denotes the embedding size used for adapter training.

Table 1: Per-class performance (%) of the SVM adapter with MedImageInsight embeddings

Class	Precision	Recall	F1	AUC
ETTube	63.0	25.4	36.3	89.8
NGTube	69.2	79.2	73.9	91.3
Pneumoperitoneum	85.9	61.8	71.9	94.6
Pneumothorax	68.4	51.4	58.7	95.3
RFrac	90.3	77.3	83.3	96.9
VLine	71.1	76.0	73.5	91.0
NormalStudy	75.5	90.0	82.1	98.1

* ETTube=endotracheal tube, NGTube=nasogastric tube, RFrac=rib fracture, VLine=vascular lines.

competitive results, frequently trailing SVM by only a small margin. In contrast, KNN and LR generally exhibited lower performance, particularly when paired with weaker embeddings. Overall, the performance gap among adapter models was much smaller than the disparity observed among embeddings.

The combination of MedImageInsight embeddings with an SVM adapter achieved the best overall performance. Detailed per-class results for this combination are presented in Table 1, with mAUC values exceeding 90% in six of the seven diagnostic categories. NormalStudy achieved the highest mAUC (98.1%) and F1 score (82.1%), while ETTube proved the most challenging, with a low recall (25.4%) and F1 score (36.3%), reflecting frequent misclassifications. The confusion matrix in Fig. 5 further reveals several notable misclassification patterns. Misclassification of ETTube as NGTube represents the largest single source of error (42.1%), with a further 21.9% of ETTube cases confused with VLine. Substantial bidirectional confusion also arises between NGTube and VLine (15.3% versus 17.9%, respectively). Moreover, 15.7% of Pneumoperitoneum and 21.9% of Pneumothorax instances are incorrectly classified as NGTube, indicating that the model occasionally interprets radiographic features of pathological air collections as tube structures. Overall, these patterns highlight the difficulty in differentiating visually similar lines and tubes (e.g., ETTube, NGTube, and VLine) on chest radiographs, suggesting that finer-grained radiographic features are crucial for accurate classification.

In addition to accuracy, fairness analysis was conducted to assess the model’s equitable performance across gender and age groups for different adapters trained on MedImageInsight embeddings. The performance differences between female (F) and male (M) groups were minimal across all adapter models, as demonstrated by the mAUC difference

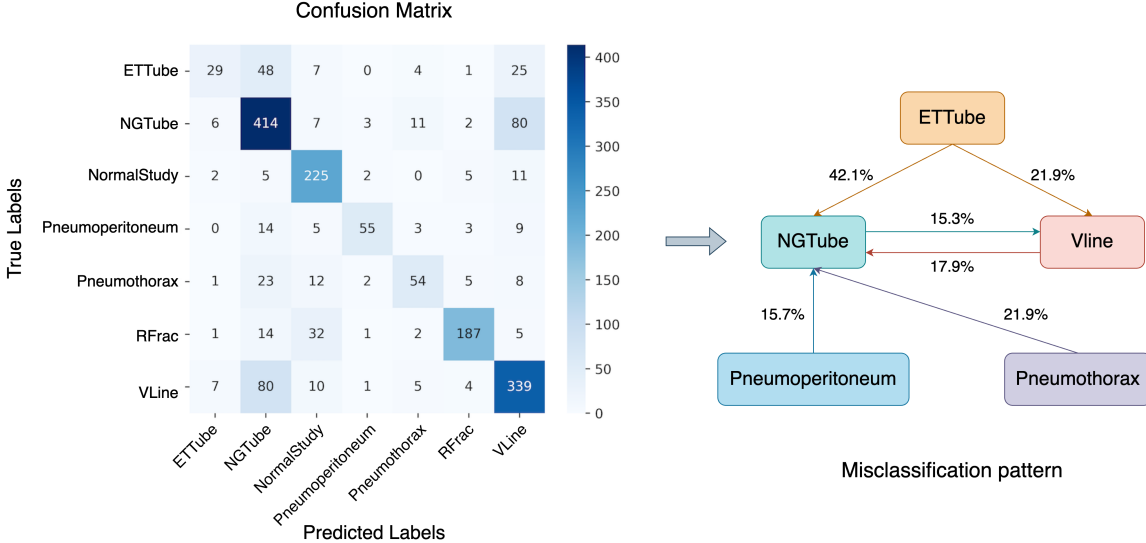


Figure 5: Confusion matrix (left) and corresponding misclassification pattern diagram (right) for multi-class radiographic image classification using MedImageInsight embeddings paired with an SVM adapter. The confusion matrix illustrates counts of predictions versus true labels, highlighting correctly classified samples along the diagonal and misclassifications off-diagonal. The misclassification pattern diagram indicates prevalent confusion among specific classes, with arrow directions representing the direction of misclassification and percentages denoting the proportion of misclassified cases relative to the total cases of each true class.

shown in Table 2. Specifically, gender-related differences were small, with the largest observed mAUC disparity being 2.0% (KNN), followed by SVM (0.9%), LG (0.7%), RF (1.0%), and MLP (0.3%), indicating robust and equitable predictions irrespective of gender. Furthermore, performance across age groups showed similarly consistent results as indicated in Table 3. The standard deviation (std) of mAUC scores across the five age categories remained generally low, with values ranging between 0.9% (SVM) and 2.9% (LG). Notably, higher variability was observed within specific diagnostic classes, such as Pneumothorax (up to 19.0% std for LG and 16.9% for MLP), suggesting potential areas for targeted improvements. Overall, the fairness analysis indicates that the evaluated models maintain consistent diagnostic performance across demographic subgroups, supporting equitable clinical utility.

Beyond fairness, computational efficiency was assessed through the training and inference times of each adapter model on a CPU, as summarized in Table 4. All adapters achieved fast inference times, with most completing predictions in under 0.1 seconds, reinforcing their suitability for real-time or resource-constrained clinical settings. SVM was the exception, with a longer but still acceptable inference time of 1.909 seconds. For training, KNN required negligible time (0.004 s), while LR (5.717 s) and MLP (5.147 s) provided a good balance between speed and performance. SVM (41.555 s) and RF (32.361 s) incurred higher training costs but less than one minute, remained within acceptable limits for efficient deployment.

These findings indicate that foundation model embeddings, particularly those derived from MedImageInsight, can be effectively utilized to train lightweight adapter classifiers, yielding high diagnostic accuracy while maintaining computational efficiency. The variability in performance across different foundation models highlights the importance of selecting appropriate embedding representations tailored to the specific radiographic classification task.

4 Discussion

This study evaluated the diagnostic performance and computational efficiency of lightweight adapter classifiers trained on embeddings from pre-trained foundation models for multi-class classification of radiography images, with a focus on tube placement verification. Results show that adapter models effectively utilize these embeddings, achieving high mAUC values across multiple configurations. Notably, the combination of MedImageInsight embeddings with an SVM adapter achieved an mAUC of 93.85%, outperforming all other foundation model embeddings. In contrast, MedFlamingo embeddings yielded substantially lower mAUC values, underscoring the importance of selecting embeddings that are well-aligned with the radiographic classification task.

Table 2: Gender fairness assessment of AUC performance (%) from adapters trained by MedImageInsight embeddings

Adapters	Gender	ETTube	NGTube	Pneumoperitoneum	Pneumothorax	Rrac	VLine	Normal	mAUC
KNN	F	91.2	90.1	94.5	92.6	96.2	90.1	96.4	93.0
	M	85.2	88.8	90.2	93.5	95.3	87.4	96.6	91.0
	Difference	6.0	1.3	4.3	-0.8	0.9	2.7	-0.2	2.0
LG	F	90.4	91.0	95.7	92.7	98.0	91.5	97.7	93.8
	M	89.8	89.6	93.5	95.1	96.2	90.6	97.6	93.2
	Difference	0.5	1.4	2.2	-2.4	1.8	0.9	0.1	0.7
SVM	F	92.2	91.5	94.6	94.9	98.0	91.6	98.0	94.4
	M	88.5	91.1	94.5	95.5	96.2	90.6	98.1	93.5
	Difference	3.7	0.4	0.1	-0.6	1.8	1.0	-0.1	0.9
RF	F	87.9	91.2	95.1	92.9	97.5	91.2	97.4	93.3
	M	86.5	90.0	93.4	95.0	94.7	89.7	97.0	92.3
	Difference	1.5	1.2	1.8	-2.1	2.8	1.5	0.4	1.0
MLP	F	91.7	91.1	95.4	91.3	97.7	91.7	97.9	93.8
	M	90.6	90.8	93.0	94.5	96.7	91.0	98.1	93.5
	Difference	1.1	0.3	2.3	-3.2	1.0	0.7	-0.3	0.3

* KNN = k-nearest neighbors, LG = logistic regression, SVM = support vector machine, RF = random forest, MLP = multi-layer perceptron, ETTube=endotracheal tube, NGTube=nasogastric tube, RFract=rib fracture, VLine=vascular lines, F=female patients (709 in total), M=male patients (1059 in total).

The results highlight the critical role of domain knowledge in improving classification performance. Among models trained solely on image data, Rad-DINO, which is specifically focused on radiography images, outperformed the more general DenseNet121, emphasizing the benefits of domain-focused pretraining. A similar pattern was observed among vision-language models: both BiomedCLIP and Med-Flamingo, trained on biomedical image-text pairs from scientific articles, achieved moderate performance but were outperformed by models trained on large-scale Chest-Xray imaging datasets, like CXR-Foundation.

An especially notable finding is the exceptional performance of MedImageInsight, despite it not being limited to radiography data. Unlike Rad-DINO and CXR-Foundation, which are tailored specifically to radiography and chest X-rays, MedImageInsight leverages data from a broad range of medical imaging modalities. This cross-modal training may enable the model to capture richer semantic features and shared medical imaging patterns, ultimately enhancing its representation power for radiographic tasks. These observations suggest that while task-specific domain adaptation is beneficial, diversity and scale across medical domains can provide additional gains, potentially offering more generalizable and semantically meaningful embeddings that transfer effectively across tasks.

Despite achieving the best overall performance, the MedImageInsight + SVM combination struggled to distinguish between ETTube, NGTube, and VLine, as evidenced by the confusion matrix in Fig. 5. This issue is also apparent in the t-SNE visualization of MedImageInsight embeddings shown in Fig. 3, where these three classes are not clearly separated compared to others. Such overlap suggests that while the foundation model captures general semantic features, it may not preserve the fine-grained details needed to differentiate visually similar tube placements. These findings highlight a limitation of current multi-modal foundation models in retaining subtle cues critical for tasks involving highly similar anatomical structures or device orientations.

In the fairness analysis of MedImageInsight embeddings, the performance differences between genders across all adapters were minimal, with the largest observed gap being just 2.0%. Similarly, the variability across age groups was modest, with a maximum difference of 2.9%. However, a noticeable performance decrease was identified for the senior age group (80–100 years) within the Pneumothorax diagnostic class, particularly when using LG and MLP adapters, only 53.5% and 58.0% respectively shown in Table 3. This reduction may be attributable to the limited senior Pneumothorax patients in the test dataset, only three patients, suggesting more data are needed for accurate performance estimation.

The results of our investigation provide compelling evidence that foundation model embeddings, especially those derived from domain-specific models such as MedImageInsight, can be harnessed to train efficient and accurate adapter classifiers. The observed superiority of the SVM adapter across most configurations further emphasizes the potential of combining pre-trained embeddings with lightweight, traditional machine learning classifiers[16, 17]. Moreover, the computational efficiency demonstrated—where training and inference times remained within seconds for most models

Table 3: Age fairness assessment of AUC performance (%) from adapters trained by MedImageInsight embeddings

Adapters	Age	ETTube	NGTube	Pneumoperitoneum	Pneumothorax	Rrac	VLine	Normal	mAUC
KNN	(0, 20]	98.7	84.3	100.0	99.1	100.0	79.3	99.7	94.4
	(20, 40]	85.8	89.1	77.3	90.9	96.8	88.2	97.1	89.3
	(40, 60]	86.7	91.0	92.7	94.9	95.5	90.0	97.3	92.6
	(60, 80]	86.7	87.6	92.2	91.9	96.2	88.9	93.7	91.0
	(80, 100]	92.9	86.2	95.5	86.3	96.3	85.4	98.1	91.5
	std	5.5	2.6	8.5	4.8	1.8	4.3	2.2	1.9
LG	(0, 20]	100.0	87.2	100.0	99.3	99.7	84.3	100.0	95.8
	(20, 40]	91.1	91.1	93.9	91.9	98.5	91.4	97.9	93.7
	(40, 60]	87.4	90.8	94.7	96.0	97.3	91.4	98.2	93.7
	(60, 80]	90.4	88.4	92.8	95.1	97.3	90.7	96.0	93.0
	(80, 100]	94.3	87.3	97.0	53.5	96.3	92.0	96.3	88.1
	std	4.8	1.9	2.9	19.0	1.3	3.2	1.6	2.9
SVM	(0, 20]	100.0	85.6	100.0	99.4	99.9	82.8	100.0	95.4
	(20, 40]	87.5	90.4	93.7	94.7	97.9	90.5	98.2	93.3
	(40, 60]	87.3	91.4	94.9	94.8	97.5	91.4	98.8	93.7
	(60, 80]	91.1	90.9	93.4	95.1	97.4	91.6	96.5	93.7
	(80, 100]	97.0	86.8	96.4	84.7	96.8	91.8	97.3	93.0
	std	5.7	2.6	2.7	5.4	1.2	3.8	1.3	0.9
RF	(0, 20]	99.3	87.8	100.0	99.3	100.0	85.0	100.0	95.9
	(20, 40]	87.7	89.9	93.0	95.1	97.2	90.5	97.3	93.0
	(40, 60]	83.7	91.3	94.6	95.2	96.7	90.5	98.2	92.9
	(60, 80]	86.8	89.1	92.0	92.2	97.3	91.1	95.1	92.0
	(80, 100]	92.5	87.9	99.5	80.0	94.2	93.4	96.8	92.0
	std	6.1	1.5	3.7	7.3	2.1	3.1	1.8	1.6
MLP	(0, 20]	100.0	86.9	100.0	99.6	99.7	84.6	100.0	95.8
	(20, 40]	91.0	92.1	93.7	90.0	98.9	91.9	98.2	93.7
	(40, 60]	87.8	91.7	93.5	95.4	97.2	91.0	98.6	93.6
	(60, 80]	92.1	89.6	92.7	94.5	97.3	91.8	96.8	93.5
	(80, 100]	94.9	87.4	96.1	58.0	95.9	91.3	97.0	88.6
	std	4.6	2.4	3.0	16.8	1.5	3.1	1.3	2.7

* ETTube = endotracheal tube, NGTube = nasogastric tube, Rfrac = rib fracture, VLine = vascular lines, std = standard deviation. A total of 154 patients with age in the range of (0, 20], 237 patients with age in the range of (20, 40], 570 patients with age in the range of (40, 60], 610 patients with age in the range of (60, 80], and 99 patients with age in the range of (80, 100] are involved in the analysis. Patients older than 100 are unidentified and are excluded from analysis.

Table 4: Average training and inference times (in seconds) on CPU for each adapter model

Adapters	KNN	LR	SVM	RF	MLP
Training	0.004	5.717	41.555	32.361	5.147
Inference	0.048	0.003	1.909	0.096	0.006

* KNN= K-Nearest Neighbors; LR=Logistic Regression; SVM=Support Vector Machines; RF=Random Forest; MLP=Multi-Layer Perceptron

and under one minute even for the more computationally demanding classifiers—supports the feasibility of integrating these methods into clinical workflows where rapid decision-making is essential.

Despite these promising findings, several limitations must be acknowledged. Although the dataset encompassed a diverse range of clinical scenarios pertinent to tube placement, future studies should aim to validate these findings in prospective cohorts and across different clinical settings. Additionally, while our study focused mainly on tube placement verification—a task of significant clinical relevance—further research is warranted to assess the applicability of this methodology to other radiographic classification challenges.

5 Conclusion

In summary, our investigation demonstrates that foundation model embeddings, particularly those from domain-specific sources such as MedImageInsight, can be effectively employed to train lightweight adapter models for multi-class radiography classification with gender and age fairness. The high diagnostic accuracy and computational efficiency observed in this study underscore the potential of this approach to enhance clinical radiographic assessment, particularly in environments where rapid and reliable interpretation is critical. Future studies should further explore the integration of such models into clinical practice and assess their impact on diagnostic workflows and patient outcomes.

Acknowledgments

This work was supported in part by the Department of Radiology at the University of Wisconsin-Madison.

Declarations

Ethics Approval Due to the retrospective nature of the study, a waiver of informed consent was obtained.

Conflict of Interest NCFC, JM, MPL, ASP, NS, AE, CB are employees of Microsoft. NCFC holds diverse investments in the technology and healthcare sectors. John W. Garrett is an advisor to RadUnity. He and Joshua D. Warner are shareholders in NVIDIA. The remaining authors declare no competing interests.

References

- [1] Chaoyi Wu, Xiaoman Zhang, Ya Zhang, Yanfeng Wang, and Weidi Xie. Towards generalist foundation model for radiology by leveraging web-scale 2d&3d medical data. *arXiv preprint arXiv:2308.02463*, 2023.
- [2] Emily Keyte, Gillian Roe, Annmarie Jeanes, and Jeannette K Kraft. Immediate chest radiograph interpretation by radiographers improves patient safety related to nasogastric feeding tube placement in children. *Pediatric Radiology*, 51:1621–1625, 2021.
- [3] Carena D McMullen, Chris Anstey, Peter Garrett, and John Moore. Nasogastric tube placement under sonographic observation: A comparison study of ultrasound and chest radiography in mechanically ventilated patients. *Australian Critical Care*, 35(2):181–185, 2022.
- [4] IMV. 2021 X-ray DR CR Market Outlook Report. Technical report, IMV Medical Information Division, 2021. Accessed: March 31, 2023.
- [5] BS Kelly, C Judge, SM Bolland, SM Clifford, GM Healy, A Aziz, P Mathur, S Islam, KW Yeom, A Lawlor, and RP Killeen. Radiology artificial intelligence: a systematic review and evaluation of methods (raise). *European Radiology*, 32(11):7998–8007, 2022.
- [6] C Mello-Thoms and CAB Mello. Clinical applications of artificial intelligence in radiology. *British Journal of Radiology*, 96(1150):20221031, 2023.
- [7] R Najjar. Redefining radiology: A review of artificial intelligence integration in medical imaging. *Diagnostics (Basel)*, 13(17):2760, 2023.
- [8] David M Knigge, David W Romero, Albert Gu, Efstratios Gavves, Erik J Bekkers, Jakub Mikolaj Tomczak, Mark Hoogendoorn, and Jan-jakob Sonke. Modelling long range dependencies in n d: From task-specific to a general purpose cnn. In *The Eleventh International Conference on Learning Representations*.
- [9] Kaoutar Ben Ahmed, Gregory M Goldgof, Rahul Paul, Dmitry B Goldgof, and Lawrence O Hall. Discovery of a generalization gap of convolutional neural networks on covid-19 x-rays classification. *Ieee Access*, 9:72970–72979, 2021.
- [10] Ahmad Waleed Salehi, Shakir Khan, Gaurav Gupta, Bayan Ibrahim Alabdullah, Abrar Almjally, Hadeel Alsolai, Tamanna Siddiqui, and Adel Mellit. A study of cnn and transfer learning in medical imaging: Advantages, challenges, future scope. *Sustainability*, 15(7):5930, 2023.
- [11] Michael Moor, Oishi Banerjee, Zahra Shakeri Hossein Abad, Harlan M Krumholz, Jure Leskovec, Eric J Topol, and Pranav Rajpurkar. Foundation models for generalist medical artificial intelligence. *Nature*, 616(7956):259–265, 2023.

- [12] Ce Zhou, Qian Li, Chen Li, Jun Yu, Yixin Liu, Guangjing Wang, Kai Zhang, Cheng Ji, Qiben Yan, Lifang He, et al. A comprehensive survey on pretrained foundation models: A history from bert to chatgpt. *International Journal of Machine Learning and Cybernetics*, pages 1–65, 2024.
- [13] Muhammad Awais, Muzammal Naseer, Salman Khan, Rao Muhammad Anwer, Hisham Cholakkal, Mubarak Shah, Ming-Hsuan Yang, and Fahad Shahbaz Khan. Foundation models defining a new era in vision: a survey and outlook. *IEEE Transactions on Pattern Analysis and Machine Intelligence*, 2025.
- [14] Alec Radford, Jong Wook Kim, Chris Hallacy, Aditya Ramesh, Gabriel Goh, Sandhini Agarwal, Girish Sastry, Amanda Askell, Pamela Mishkin, Jack Clark, et al. Learning transferable visual models from natural language supervision. In *International conference on machine learning*, pages 8748–8763. PMLR, 2021.
- [15] Sheng Zhang, Yanbo Xu, Naoto Usuyama, Hanwen Xu, Jaspreet Bagga, Robert Tinn, Sam Preston, Rajesh Rao, Mu Wei, Naveen Valluri, Cliff Wong, Andrea Tupini, Yu Wang, Matt Mazzola, Swadheen Shukla, Lars Liden, Jianfeng Gao, Angela Crabtree, Brian Piening, Carlo Bifulco, Matthew P. Lungren, Tristan Naumann, Sheng Wang, and Hoifung Poon. A multimodal biomedical foundation model trained from fifteen million image–text pairs. *NEJM AI*, 2(1), 2024.
- [16] M Paschali, Z Chen, L Blankemeier, M Varma, A Youssef, C Bluethgen, C Langlotz, S Gatidis, and A Chaudhari. Foundation models in radiology: What, how, why, and why not. *Radiology*, 314(2):e240597, 2025.
- [17] MJ Willemink, HR Roth, and V Sandfort. Toward foundational deep learning models for medical imaging in the new era of transformer networks. *Radiology: Artificial Intelligence*, 4(6):e210284, 2022.
- [18] AB Sellergren, C Chen, Z Nabulsi, Y Li, A Maschinot, A Sarna, J Huang, C Lau, SR Kalidindi, M Etemadi, F Garcia-Vicente, D Melnick, Y Liu, K Eswaran, D Tse, N Beladia, D Krishnan, and S Shetty. Simplified transfer learning for chest radiography models using less data. *Radiology*, 305(2):454–465, 2022.
- [19] Noel CF Codella, Ying Jin, Shrey Jain, Yu Gu, Ho Hin Lee, Asma Ben Abacha, Alberto Santamaría-Pang, Will Guyman, Naiteek Sangani, Sheng Zhang, et al. Medimageinsight: An open-source embedding model for general domain medical imaging. *arXiv preprint arXiv:2410.06542*, 2024.
- [20] Gao Huang, Zhuang Liu, Laurens Van Der Maaten, and Kilian Q Weinberger. Densely connected convolutional networks. In *Proceedings of the IEEE conference on computer vision and pattern recognition*, pages 4700–4708, 2017.
- [21] Michael Moor, Qian Huang, Shirley Wu, Michihiro Yasunaga, Yash Dalmia, Jure Leskovec, Cyril Zakka, Eduardo Pontes Reis, and Pranav Rajpurkar. Med-flamingo: a multimodal medical few-shot learner. In *Machine Learning for Health (ML4H)*, pages 353–367. PMLR, 2023.
- [22] F Pérez-García, H Sharma, S Bond-Taylor, K Bouzid, V Salvatelli, M Ilse, S Bannur, DC Castro, A Schwaighofer, MP Lungren, MT Wetscherek, N Codella, SL Hyland, J Alvarez-Valle, and O Oktay. Exploring scalable medical image encoders beyond text supervision. *Nature Machine Intelligence*, 7(1):119–130, 2025.
- [23] Ross Wightman. Pytorch image models. <https://github.com/rwightman/pytorch-image-models>, 2019.
- [24] Microsoft. Biomedclip-pubmedbert_256-vit_base_patch16_224, 2025. Available at: https://huggingface.co/microsoft/BiomedCLIP-PubMedBERT_256-vit_base_patch16_224.
- [25] Google. Cxr-foundation, 2025. Available at: <https://huggingface.co/google/cxr-foundation>.
- [26] Team MF. Med-flamingo, 2025. Available at: <https://huggingface.co/med-flamingo/med-flamingo>.
- [27] Microsoft. Medimageinsight, 2025. Available at: <https://huggingface.co/lion-ai/MedImageInsights>.
- [28] Microsoft. Rad-dino, 2025. Available at: <https://huggingface.co/microsoft/rad-dino>.
- [29] Laurens Van der Maaten and Geoffrey Hinton. Visualizing data using t-sne. *Journal of machine learning research*, 9(11), 2008.
- [30] F Pedregosa, G Varoquaux, A Gramfort, V Michel, B Thirion, O Grisel, M Blondel, P Prettenhofer, R Weiss, V Dubourg, J Vanderplas, A Passos, D Cournapeau, M Brucher, M Perrot, and E Duchesnay. Scikit-learn: Machine learning in python. *Journal of Machine Learning Research*, 12:2825–2830, 2011.